Auton Robot (2008) 24: 419–434
DOI 10.1007/s10514-008-9088-5

Development of a compliance controller to reduce energy consumption for bipedal robots

Bram Vanderborght · Björn Verrelst · Ronald Van Ham · Michaël Van Damme · Pieter Beyl · Dirk Lefeber

Received: 12 August 2007 / Accepted: 23 January 2008 / Published online: 6 February 2008

Abstract In this paper a strategy is proposed to combine active trajectory tracking for bipedal robots with exploiting the natural dynamics by simultaneously controlling the torque and stiffness of a compliant actuator. The goal of this research is to preserve the versatility of actively controlled humanoids, while reducing their energy consumption. The biped Lucy, powered by pleated pneumatic artificial muscles, has been built and controlled and is able to walk up to a speed of 0.15 m/s. The pressures inside the muscles are controlled by a joint trajectory tracking controller to track the desired joint trajectories calculated by a trajectory generator. However, the actuators are set to a fixed stiffness value. In this paper a compliance controller is presented to reduce the energy consumption by controlling the stiffness. A mathematical formulation has been developed to find an optimal stiffness setting depending on the desired trajectory and physical properties of the system and the proposed strategy has been validated on a pendulum structure powered by artificial muscles. This strategy has not been implemented on the real robot because the walking speed of the robot is currently too slow to benefit already from compliance control.

Keywords Biped · Pneumatic artificial muscle · Torque and compliance control · Energy-efficient walking

B. Vanderborght (✉) · B. Verrelst · R. Van Ham · M. Van Damme · P. Beyl · D. Lefeber
Department of Mechanical Engineering, Vrije Universiteit Brussel, Pleinlaan 2, 1050 Brussel, Belgium
e-mail: bram.vanderborght@vub.ac.be

B. Vanderborght
Robotics, Brain and Cognitive Sciences Department, Italian Institute of Technology, Via Morego 30, 16163 Genova, Italy

1 Introduction

An important deficiency of walking robots in comparison with their biological counterparts is the high power consumption. The continuous operating time of for example Asimo is 1 hour (Honda Motor Co., Ltd. 2005). In order to ever be useful in a real application the autonomy must definitely increase. This can be done by developing better power sources (e.g. batteries) and increasing the efficiency of walking. The most energy efficient bipeds are the so called passive walkers, they don't need any actuation at all to walk down a slope. The slope is used as a source of energy to compensate the friction and impact losses. By using compliant actuators these robots can walk on level ground. The energetic cost (amount of energy used per meter traveled per unit of weight) of these robots is between one and two orders of magnitude smaller than the energetic cost of actively controlled humanoids (Collins et al. 2005).

The passive walkers are designed to exploit the natural dynamics of the system while walking. Unfortunately they are of little practical use: they cannot start and stop autonomously and they cannot change their gait due to the fixed dynamics. This is in contrast with the actively controlled bipeds as for example Asimo and HRP-2. They use precise joint-angle control and are consequently very versatile. For example these robots are able to walk among obstacles (Michel et al. 2005), step over obstacles (Verrelst et al. 2006a), climb stairs (Kajita et al. 2003) and manipulate objects while walking (Yoshida et al. 2006). These capabilities are still impossible for the actuated passive walkers. The optimum is probably somewhere in between the active and passive walkers as shown in Fig. 1: a combination of active control to be able to perform different tasks with exploiting the passive dynamics to reduce energy consumption. Most of the research trying to incorporate energy ef-

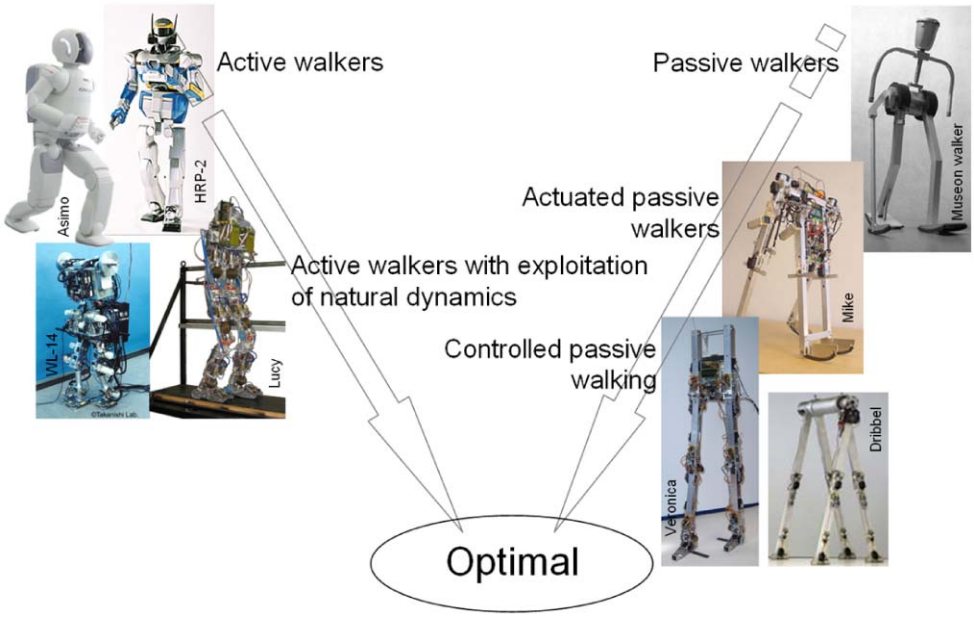

Fig. 1 Location of the biped Lucy among the active and passive bipeds

ficient locomotion is performed on the side of the passive walkers. On the other hand, the active robots are usually built to evaluate task driven applications with as final goal to have enough capabilities for close cooperation with humans in a home or office. The goal of the Lucy project is to investigate how actively controlled robots can improve their energy efficiency while maintaining their versatility. Consequently this work is situated on the side of the active walkers. The proposed control strategy is a combination of calculating dynamically stable trajectories for the different joint links which are tracked by actively controlling the actuators in the different joints and an extra controller to reduce the energy consumption. Essential for this research is the use of adaptable compliant actuators so the natural dynamics of the system can be controlled. Adaptable compliance is also important for human walking and running. Electromyograhical data shows there is little muscle activity during for instance the swing phase of the leg in walking (Basmajian and De Luca 1985). So this motion is mainly passive. In running, kinetic energy is stored in the Achilles tendon and released in the next hop (Ferris and Farley 1997). The compliant actuators also allow to absorb the energy released during impact shocks. An interesting actuator, introducing such compliance for robotic mechanisms, is the pleated pneumatic artificial muscle (PPAM, Verrelst et al. 2006b), because in an antagonistic setup both the torque and the compliance of the joint can be controlled.

The robot Lucy (Fig. 2, Verrelst et al. 2005) is powered by 12 PPAM's to actuate 6 DOF: the hip, knee and ankle of both legs. It is a planar walking robot, a guiding mechanism prevents the robot from falling sidewards. The guiding mechanism consists of a horizontal and vertical rail. Because the rails have limited length a treadmill is used to be able to walk longer distances.

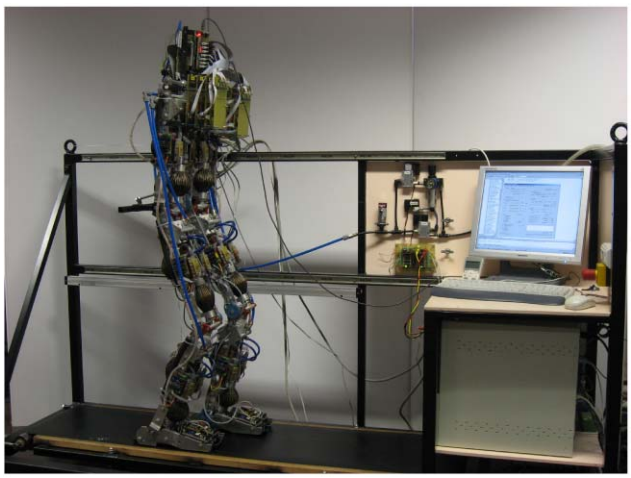

Fig. 2 Biped Lucy on treadmill with computer

The control strategy starts from dynamically stable trajectories generated by the trajectory generator. The joint trajectory tracking controller controls the pressures inside the muscles so the desired motion is followed. At this moment the compliance setting is fixed. A compliance controller, as discussed in this paper, can improve the performances of the robot regarding the energy consumption. The current maximum walking speed of the robot is 0.15 m/s which makes the robot the fastest in the group of trajectory controlled pneumatic bipeds. Please go to http://lucy.vub.ac.be/phdlucy.wmv to watch a video of the biped Lucy. The number of pneumatic bipeds robots built worldwide up till now is rather limited compared to the amount of robots with elec-

trical actuation. The main reason is that the control of pneumatics is much more difficult. One of the first to incorporate pneumatics is the Japanese pioneer of walking bipeds Kato. During the sixties and seventies he has built several statically balanced walking bipeds such as WAP I, II and III (Kato et al. 1972). Guihard et al. designed BIPMAN (Gorce and Guihard 1998) and the Shadow Walker is a wooden leg-skeleton powered by Shadow air muscles and built by the Shadow Company (Walker 1996). Spampinato and Muscato constructed a 10 DOF biped actuated by pneumatic pistons (Guccione et al. 2003). The group of Caldwell, at the university of Salford, developed the biped Salford Lady (Caldwell et al. 1997) actuated with McKibben artificial muscles.

The idea of using compliance is a fairly new concept in robotics, for a long period the suggestion was "the stiffer the better". Now researchers are working on strategies to benefit from non-stiff actuation. Some researchers want to use it for a safe human-robot interaction (Bicchi et al. 2003). This paper is devoted to reducing energy consumption by exploiting the natural dynamics of the system. This research has been carried out on a pendulum set-up actuated by an antagonistic pair of pleated pneumatic artificial muscles. The design is exactly the same as the limbs of the robot Lucy.

Why study a pendulum motion for reducing the energy consumption? Walking is often modeled as the motion of two coupled pendula, because the stance leg behaves like an inverted pendulum moving about the stance foot, and the swing leg like a regular pendulum swinging about the hip (Kuo et al. 2005). When given an initial push, a simple gravity pendulum will swing back and forth under the influence of gravity at a certain frequency. The swing amplitude will gradually decrease due to the friction losses. When the pendulum is powered by an electrical motor a controller is able to follow the same trajectory as the freely swinging pendulum.

The advantage of the first approach is that, if friction is neglected, the pendulum motion consumes no energy. It is however obvious that using the second approach, the pendulum is able to track whatever desired trajectory, of course within the limits of the controller and generally requiring more energy. If the pendulum is equipped with a torsion spring the pendulum will oscillate at a higher frequency, but still only at a fixed frequency. If the pendulum is powered by an actuator with adaptable passive compliance different resonant frequencies can be selected. This is the main idea behind having minimal energy consumption with different desired trajectories: controlling the compliance to select an appropriate natural motion while applying torques to deviate the trajectory from the unforced swing motion.

In Sect. 2 the pendulum is presented together with the force characteristic of a PPAM and the torque and compliance characteristic of an antagonistic muscle setup. First sinusoidal functions as imposed trajectories are studied on the real pendulum. These motions are studied first in Sect. 3, because they resemble the natural unforced motion of a pendulum. The results show that for a certain frequency an optimal compliance can be found for which the airmass consumption is minimal. At this optimal compliance the number of valve actions is strongly reduced. A mathematical formulation is proposed in Sect. 4 to calculate the optimal compliance depending on the physical properties of the pendulum and the frequency of the imposed trajectory. The idea of the formulation is to fit the controllable actuator compliance to the "natural" compliance of the desired trajectory, and combine that with trajectory tracking control. This means that the torque of the joint is calculated so a desired trajectory is tracked, while the compliance is calculated to reduce the energy consumption. For a sinusoidal function with small angles the "natural" compliance of the desired trajectory is a constant over the trajectory. For more complex trajectories this is not the case anymore. Therefore, Sect. 5 is dedicated to the development of a suitable strategy for all trajectories. This section builds on previous experiments by Vanderborght et al. (2006b), where only sinusoidal functions were discussed.

In this paper experimental results and simulations alternate. In every caption it is mentioned by "real" and "sim" whether the graphs have been taken from real experiments or have been obtained by means of simulations respectively.

2 Pendulum powered by PPAMs

The complete pendulum set-up is shown in Fig. 3. The physical properties of the pendulum are:

- Length of the link: $l = 0.45$ m
- Coefficient denoting COG from rotating joint: $\alpha = 0.77$
- Mass: $m = 6.81$ kg
- Inertia in COG: $I = 0.1105\ \text{kg}\,\text{m}^2$
- Joint angle range: $\theta_{min} = -35$, $\theta_{max} = 35°$

The sensors are an Agilent HEDM6540 incremental encoder for reading the joint position and two pressure sensors (Honeywell CPC100AFC), mounted inside each muscle. The controller is implemented on a PC and 2 data acquisition cards of National Instruments are used. The NI PCI-6602 Counter/Timer with 8 up/down, 32-bit counter/timers is used to measure the joint angles and a NI PCI-6220 with 16 analog inputs and 24 digital I/O are used to control the valves, measure the pressures and joint velocity. Both PC cards are unable to infer the angular velocity from the encoder signal, so a PIC16F876A micro-controller, working at 2 MHz is used to measure the time between the pulses and detect the sign. The velocity signal is sent as an analog signal to the data acquisition card. The airmass consumption is measured by a compressed air meter (IFM Electronics SD6000).

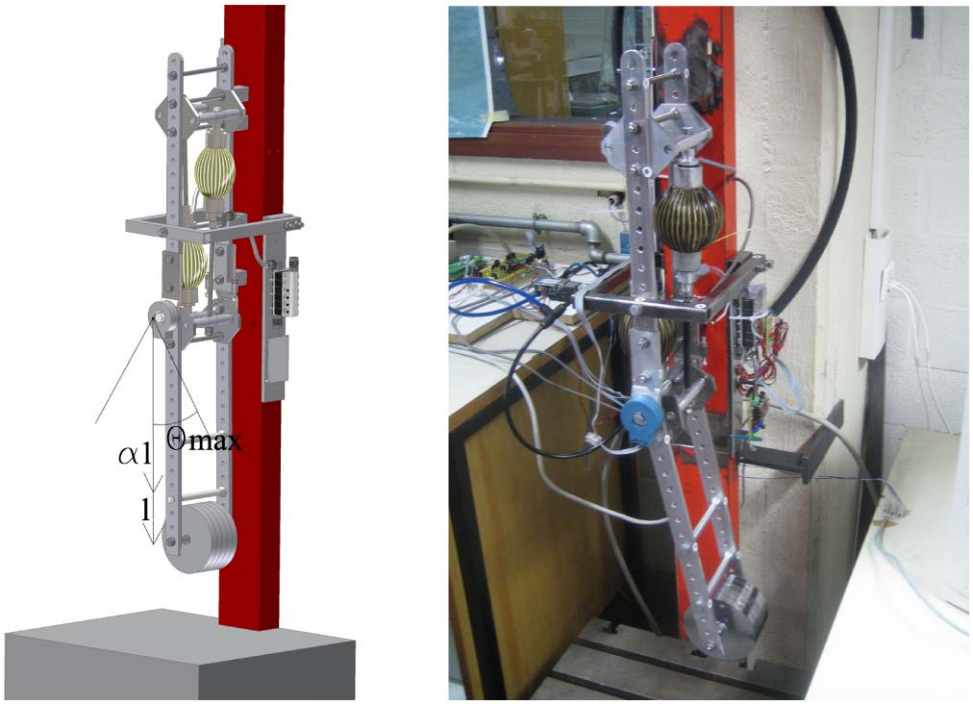

Fig. 3 CAD drawing and photograph of the physical pendulum

2.1 Force characteristics of pleated pneumatic artificial muscles

A pneumatic artificial muscle is essentially a membrane that expands radially and contracts axially when inflated, while generating high pulling forces along the longitudinal axis. Different designs have been developed. The best known is the so called McKibben muscle (Schulte 1961). This muscle contains a rubber tube which expands when inflated, while a surrounding netting transfers tension. Hysteresis, mainly due to dry friction between the netting and the rubber tube, makes control of such a device rather complicated. Typical for this type of muscle is a threshold level of pressure before any action can take place. The main goal of the Pleated Pneumatic Artificial Muscle (PPAM) design (Daerden and Lefeber. 2001) was to avoid friction, thus making control easier by avoiding the threshold and reducing hysteresis. This was achieved by arranging the membrane into radially laid out folds that can unfurl free of radial stress when inflated. Tension is transferred by longitudinal fibres that are positioned at the bottom of each crease. A photograph of different contraction levels of the PPAM is given in Fig. 4. If the influence of the elasticity of the high tensile strength material used for the fibres is omitted, the generated force is given by (Verrelst et al. 2006b):

$$F = pl^2 f\left(\epsilon, \frac{l}{R}\right) \tag{1}$$

Fig. 4 Photograph of 3 contraction levels of the PPAM

where p is the applied gauge pressure, l the muscle's full length, R its unloaded radius and ϵ the contraction. The dimensionless force function f depends only on contraction and geometry. The graph in Fig. 5 gives the generated force for different pressures in a muscle with initial length 110 mm and initial diameter 25 mm. Forces up to 5000 N can be generated with gauge pressure of only 3 bar in a device weighing about 150 g. At low contractions, forces are extremely high causing excessive material loading, and at large contractions the generated forces drop to very low levels. So, in practice, effective contraction is limited between 5 and 35%.

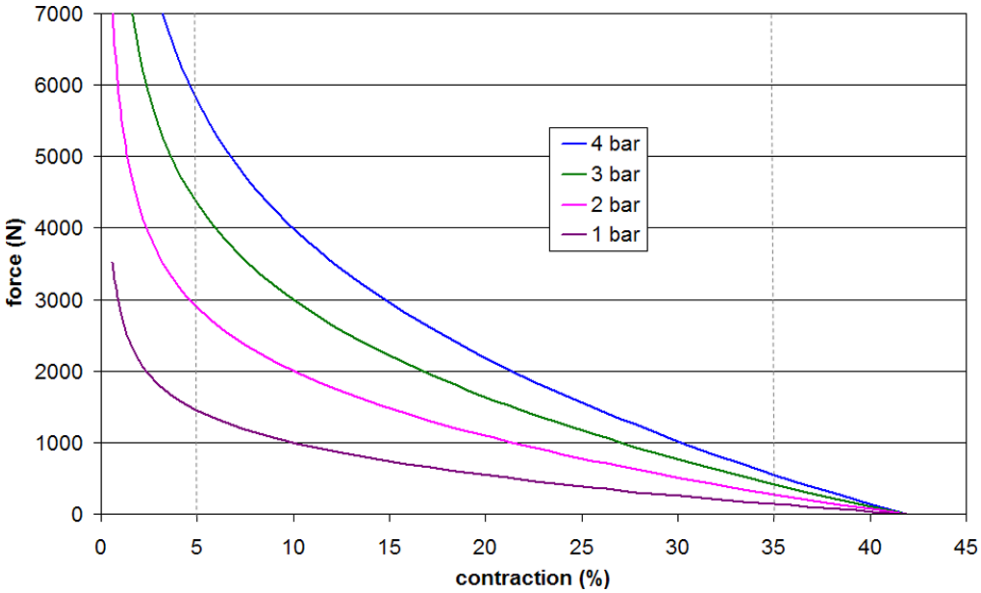

Fig. 5 Generated forces (N)

2.2 Torque characteristics of an antagonistic muscle setup

Pneumatic artificial muscles can only pull. In order to have a bidirectionally working revolute joint one has to couple two muscles antagonistically. The muscle connections—pull rods and lever mechanism—were designed in such a way the muscle's non-linear force-length characteristic is transformed to a more linear torque-angle characteristic. The dimensions of the muscles and the lever arm can be chosen in order to meet the specified joint characteristic, not only torque level but also range of motion. Taking into account equation (1) and if r_1 and r_2 define the lever arm of the agonist and antagonist muscle respectively, the joint torque is given by following expression

$$\begin{aligned} T = T_1 - T_2 &= p_1 l_1^2 r_1 f_1 - p_2 l_2^2 r_2 f_2 \\ &= p_1 t_1(\theta) - p_2 t_2(\theta) \end{aligned} \tag{2}$$

where p_1 and p_2 are the applied gauge pressures in the agonist and antagonist muscles respectively having lengths l_1 and l_2. The dimensionless force functions of both muscles are given by f_1 and f_2. The functions t_1 and t_2, in equation (2), are determined by the choices made during the design and are given by $l_1^2 r_1 f_1$ and $l_2^2 r_2 f_2$ respectively, consequently they are dependent of the joint angle θ. Thus joint position is influenced by weighted differences in the gauge pressures of both.

2.3 Compliance characteristics of an antagonistic muscle setup

Due to the gas compressibility the muscle is compliant. Joint stiffness, the inverse of compliance, for the considered revolute joint can be obtained by the angular derivative of the torque characteristic in (2):

$$\begin{aligned} K = \frac{dT}{d\theta} &= \frac{dT_1}{d\theta} - \frac{dT_2}{d\theta} \\ &= \frac{dp_1}{d\theta} t_1 + p_1 \frac{dt_1}{d\theta} - \frac{dp_2}{d\theta} t_2 - p_2 \frac{dt_2}{d\theta}. \end{aligned} \tag{3}$$

The terms $\frac{dp_i}{d\theta} t_i$ represent the stiffness due to the change of pressure with contraction, which is determined by the thermodynamical processes and the action of the pressure valves. If polytropic compression/expansion with closed valves is assumed, then the pressure changes inside the muscle will be a function of volume changes:

$$P_i V_i^n = P_{i_o} V_{i_o}^n \tag{4}$$

with:

$$P_i = P_{atm} + p_i \tag{5}$$

leading to:

$$\frac{dp_i}{d\theta} = -n \left(P_{atm} + p_{i_o} \right) \frac{V_{i_o}^n}{V_i^{n+1}} \frac{dV_i}{d\theta} \tag{6}$$

where P_i, V_i are the absolute pressure and volume of muscle i, P_{i_o} is the absolute initial pressure, V_{i_o} is the initial volume when the valves of muscle i were closed and p_i, p_{i_o} is the gauge pressure and initial gauge pressure. n is the polytropic index and P_{atm} is the atmospheric pressure. V_i and $\frac{dV_i}{d\theta}$ are determined with the fitted polynomial volume function, which gives the theoretical volume of the muscle as a function of the contraction (Verrelst et al. 2006b). The contraction is directly related to the joint angle θ determined by the pull rods and lever mechanism.

Taking the torque characteristics as an example the following reasoning can be made for muscles with closed valves. An increase of the angle θ will result in an increase of the torque generated by the agonistic muscle while its volume will decrease. Thus $dt_1/d\theta > 0$ and $dV_1/d\theta < 0$. For the antagonistic muscle the actions will be opposite. Combining (3), (4) and (6) with this information gives:

$$K = (k_1 p_{1_o} + k_2 p_{2_o} + k_{atm} P_{atm}) \tag{7}$$

with:

$$k_1 = t_1 n \frac{V_{1_o}^n}{V_1^{n+1}} \left|\frac{dV_1}{d\theta}\right| + \frac{V_{1_o}^n}{V_1^n} \left|\frac{dt_1}{d\theta}\right| > 0,$$

$$k_2 = t_2 n \frac{V_{2_o}^n}{V_2^{n+1}} \left|\frac{dV_2}{d\theta}\right| + \frac{V_{2_o}^n}{V_2^n} \left|\frac{dt_2}{d\theta}\right| > 0,$$

$$k_{atm} = k_1 + k_2 - \left|\frac{dt_1}{d\theta}\right| - \left|\frac{dt_2}{d\theta}\right|.$$

The coefficients k_1, k_2, k_{atm} are a function of the joint angle and are determined by the joint and muscles geometry. From (7) the conclusion is drawn that a passive spring element is created with an adaptable stiffness controlled by the weighted sum of both initial gauge pressures when closing the muscle.

Since stiffness depends on a sum of gauge pressures while position is determined by differences in gauge pressure, the angular position can be controlled while setting stiffness.

2.4 Control architecture

The control architecture is similar to that used for the biped Lucy (see Vanderborght et al. 2006a) and is depicted in Fig. 6.

The tracking controller consists of a computed torque controller, a delta-p unit and a pressure bang-bang controller. The computed torque controller calculates the required joint torque based on the pendulum dynamics. The delta-p unit translates these calculated torques into desired pressure levels for the two muscles of the antagonistic set-up. Finally the bang-bang controller determines the necessary valve actions to set the correct pressures in the muscles. In the next sections these control scheme building blocks are discussed in more detail.

(1) *Computed torque*: In the first module, the joint drive torques are calculated using the well known computed torque technique consisting of a feedforward part and a PID feedback loop (Slotine and Li 1991). This results in the following calculation:

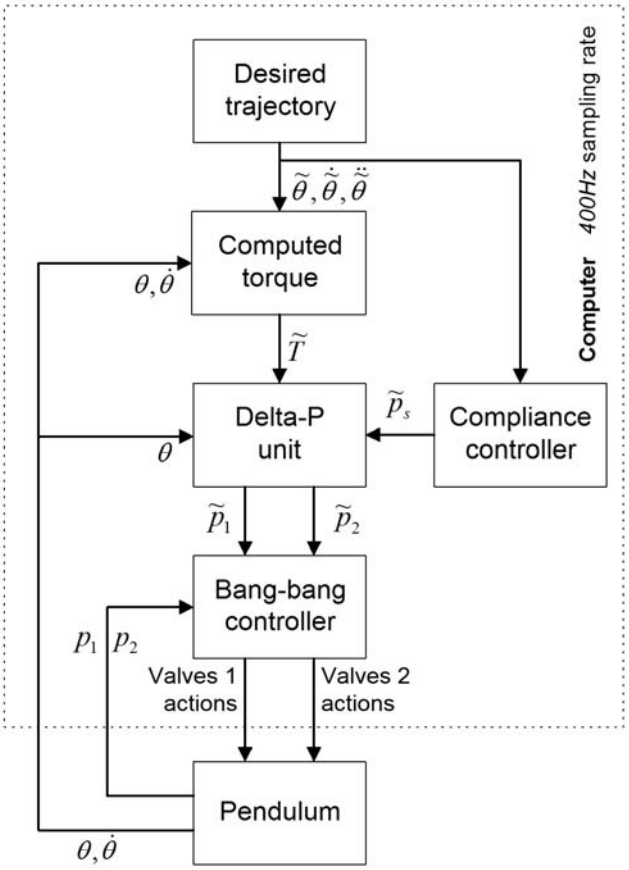

Fig. 6 Overview of the control architecture with compliance controller

$$\begin{aligned}\tilde{T} = {} & C_e(\theta, \dot{\theta})\dot{\theta} + G_e(\theta) \\ & + D_e(\theta)\Big[\ddot{\tilde{\theta}} - K_p(\theta - \tilde{\theta}) - K_i \sum(\theta - \tilde{\theta}) \\ & - K_d(\dot{\theta} - \dot{\tilde{\theta}})\Big].\end{aligned} \tag{8}$$

The parameters D_e, C_e and G_e contain the estimated values of the inertia, centrifugal, coriolis and gravitational parameters. The feedback parameters K_p, K_i and K_d are manually tuned. ˜ means desired value.

(2) *Delta-p unit*: The computed torque $\tilde{T}$ is then used as input for the delta-p control unit, which calculates the required pressure values to be set in the muscles. These two gauge pressures are generated as follows:

$$\tilde{p}_1 = \frac{\tilde{p}_s}{t_1(\tilde{\theta})} + \Delta\tilde{p}, \tag{9a}$$

$$\tilde{p}_2 = \frac{\tilde{p}_s}{t_2(\tilde{\theta})} - \Delta\tilde{p} \tag{9b}$$

with $\tilde{p}_s$ a parameter that is used to control the sum of pressures and consequently the joint stiffness and $\Delta\tilde{p}$ a parameter that controls the difference in pressure of the two muscles in order to control the generated torque. Feeding back

the joint angle θ and using expression (2), $\Delta\tilde{p}$ can be determined by:

$$\Delta\tilde{p} = \frac{\tilde{T}}{t_1(\tilde{\theta}) + t_2(\tilde{\theta})}. \tag{10}$$

The delta-p unit is thus a feed-forward calculation from torque level to pressure level and uses estimated values of the muscle force function and estimated kinematical data of the pull rod mechanism.

When (6) is substituted in (3), while using the required pressures (see (9)) for substituting p_i, then $\tilde{p}_s$ is derived as a function of the desired stiffness K.

$$\tilde{p}_s = \frac{K - g_1\Delta\tilde{p} - g_2}{g_3} \tag{11}$$

with

$$g_1(\tilde{\theta}, \dot{\tilde{\theta}}) = \left(-\frac{nt_1}{V_1}\frac{dV_1}{d\tilde{\theta}} - \frac{nt_2}{V_2}\frac{dV_2}{d\tilde{\theta}} + \frac{dt_1}{d\tilde{\theta}} + \frac{dt_2}{d\tilde{\theta}}\right),$$

$$g_2(\tilde{\theta}, \dot{\tilde{\theta}}) = P_{atm}\left(-\frac{nt_1}{V_1}\frac{dV_1}{d\tilde{\theta}} + \frac{nt_2}{V_2}\frac{dV_2}{d\tilde{\theta}}\right),$$

$$g_3(\tilde{\theta}, \dot{\tilde{\theta}}) = \left(-\frac{n}{V_1}\frac{dV_1}{d\tilde{\theta}} + \frac{n}{V_2}\frac{dV_2}{d\tilde{\theta}} + \frac{1}{t_1}\frac{dt_1}{d\tilde{\theta}} - \frac{1}{t_2}\frac{dt_2}{d\tilde{\theta}}\right).$$

Each time the controller calculates new pressures, an adaptation of $\tilde{p}_s$ should be made in order to control the compliance. The control of the compliance is consequently a feedforward calculation.

2.5 Bang-bang pressure controller

In order to realize a lightweight, rapid and accurate pressure control, fast switching on-off valves are used. The pneumatic solenoid valve 821 2/2 NC made by Matrix weighs only 25 g. The opening time is about 1 ms and it has a flow rate of 180 Std.l/ min. A set of 2 inlet and 4 outlet valves are used per muscle. In the last control block the desired gauge pressures are compared with the measured gauge pressure values after which appropriate valve actions are taken by the multi-level bang-bang pressure controller with dead zone.

3 Experimental results for sinusoidal trajectories

3.1 Airmass consumption

In a first real experiment the desired trajectory is a sine wave at a certain frequency and amplitude. The experiments have been repeated for different stiffness settings. Figures 7 and 8 show the total measured average airmass consumption over 5 swing motions as a function of the stiffness and frequency for sinusoidal trajectories with an amplitude of 5° and 10°.

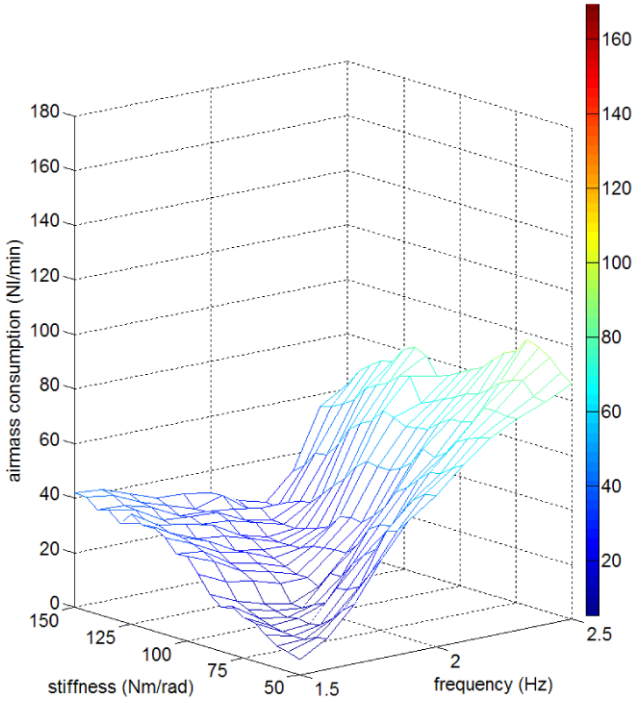

Fig. 7 Total airmass consumption vs stiffness and frequency for pendulum powered by PPAMs (sine of 5°) (real)

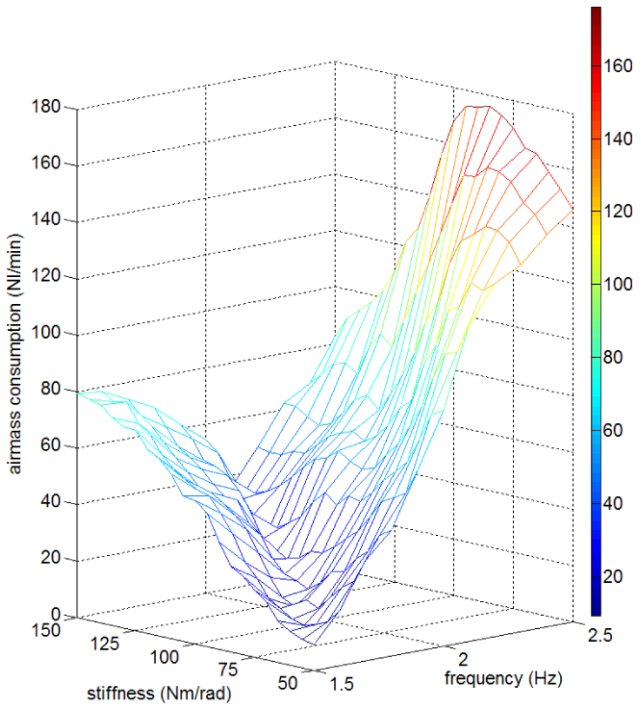

Fig. 8 Total airmass consumption vs stiffness and frequency for pendulum powered by PPAMs (sine of 10°) (real)

The frequency ranges from 1.5 Hz to 2.5 Hz, in steps of 0.1 Hz, the stiffness goes from 50 N m/rad to 150 N m/rad in steps of 5 N m/rad. The stiffness is limited because of

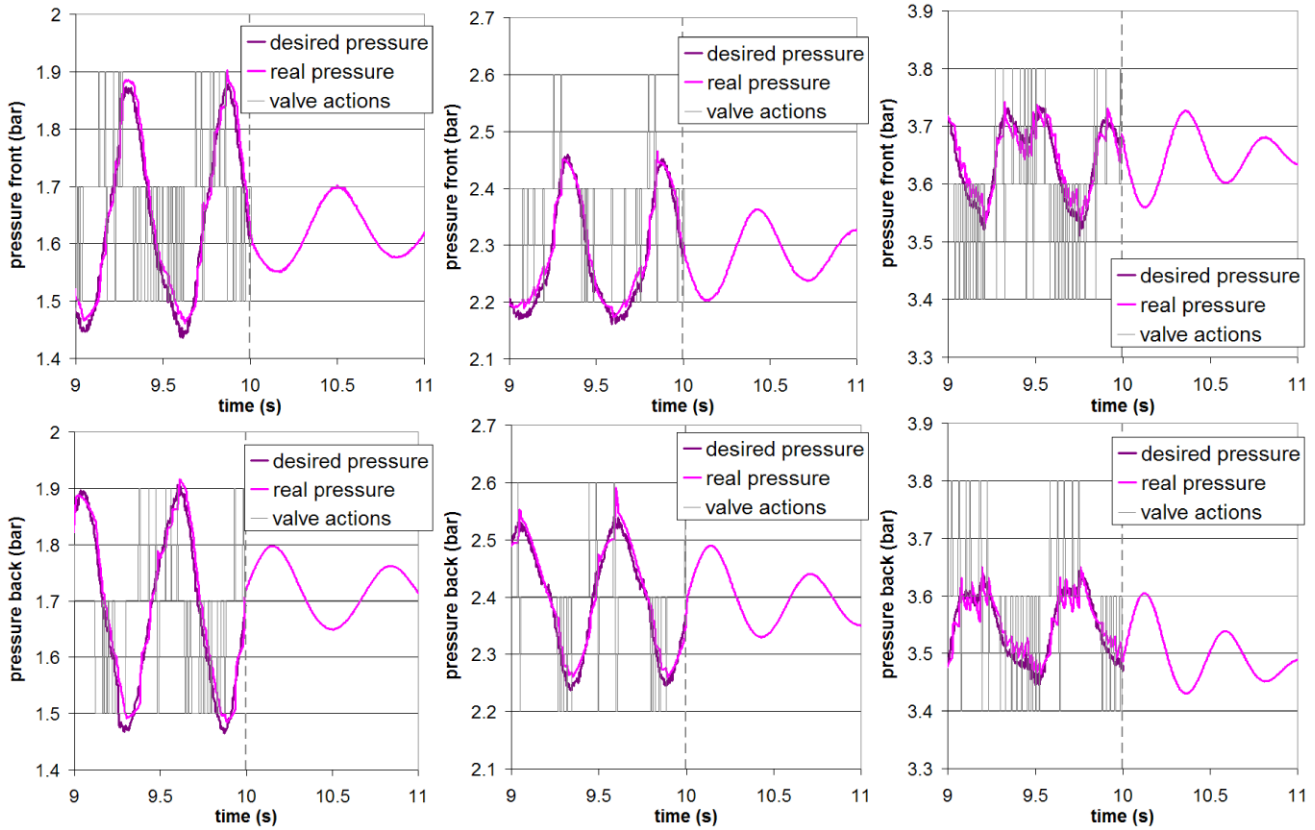

Fig. 9 Valve action and detail of the pressure courses in front and back muscle for optimal (*middle*: 85 N m/rad) and non optimal (*left*: 50 N m/rad, *right*: 150 N m/rad) stiffness setting (real)

the minimum and maximum pressure inside the muscles. At higher and lower stiffness settings the required torques cannot be generated anymore and the tracking performance deteriorates. This can be seen in (9). $\Delta\tilde{p}$ has a certain range to attain the desired torque, consequently $\tilde{p}_s$ is limited. It is clear that there exists an optimal stiffness value and it is logical that for increasing frequencies the optimal stiffness will increase as well. When the two amplitudes are compared, the optimal stiffness stays nearly the same as expected for a pendulum. The airmass consumption is however higher for larger amplitudes. The actual passive trajectory of the pendulum deviates from a pure sine-wave. This deviation increases for larger amplitudes, the same applies to the friction losses. Consequently the airmass consumption will be higher.

Another important factor influencing the airmass consumption is the dead volume in the muscle and tubing. This volume has to be pressurized and depressurized without contributing to the output force. So the tubes should be made as short as possible, thus the valve system should be placed close to the muscle. Another improvement is to add material in the muscles to reduce the dead volume. Davis et al. (2003) experimented with different filler materials which gave a higher bandwidth and reduced air consumption.

3.2 Valve action

The effect of choosing the optimal stiffness (so with the lowest airmass consumption) can also be witnessed in Fig. 9, showing real experiments. These figures show the valve actions taken by the bang-bang pressure controller and the real and desired pressure course for a desired trajectory of 1.8 Hz and $A = 5°$. The stiffness on the left was 50 N m/rad, the middle 85 N m/rad and the right 150 N m/rad. Note that in these figures closed valves are represented by a horizontal line depicted at respectively 1.7, 2.4 and 3.6 bar pressure level, while a peak of 0.2 bar upwards represents one opened inlet valve, a peak of 0.2 bar downwards one opened exhaust valve. The number of valve actions is significantly lower when the stiffness setting is at the optimal value which is the situation on the middle of Fig. 9. In the optimal case the desired pressure course is nearly the natural pressure already present in the muscle. Only a few times over the trajectory an inlet valve is opened to provide a little energy to the system to overcome the friction losses and to adapt to the deviation of the natural trajectory. In the cases where the compliance setting is not optimal (right and left of Fig. 9), significantly more valve actions are required. The imposed trajectory differs a lot from the natural movement

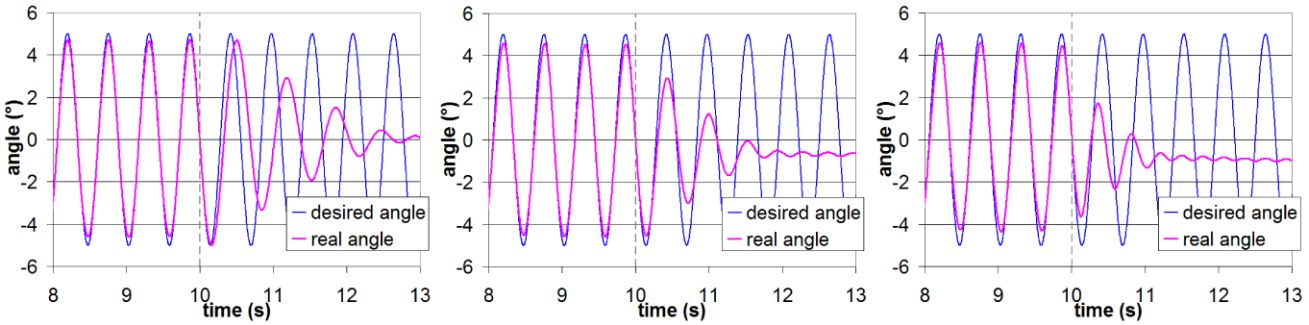

Fig. 10 Effect of closing all valves at $t = 10$ s when *left*: $K = 50$ N m/rad, *middle*: $K = 85$ N m/rad and *right*: $K = 150$ N m/rad (real)

of the pendulum causing a lot of valve switching and consequently energy dissipation. The actual motion, however, is the same because it is controlled by the joint trajectory tracking controller which can be seen in Fig. 10, showing real experiments. At $t = 10$ s the controller is stopped by closing all the valves. The pendulum, for the situation in the middle of Fig. 10 with $K = 85$ N m/rad (which is the optimal compliance for 1.8 Hz), will keep swinging with almost the same frequency as the imposed trajectory, after closing the valves. A higher stiffness compared to the optimal one means a stiffer joint, consequently the frequency increases; a lower stiffness makes the joint more compliant and thus the frequency decreases. One can see that when $K = 150$ N m/rad (Fig. 10, right), the pendulum starts oscillating after $t = 10$ s with a frequency of about 2.1 Hz, and when $K = 50$ N m/rad (Fig. 10, left) the frequency is about 1.5 Hz. These are the natural swing motion frequencies. The unforced amplitude of course decreases due to friction. The higher the pressures inside the muscles, the higher the damping. Figure 9 shows the real pressure inside the muscles after the valves are closed.

4 Compliance control

The previous experiments showed that each time an optimal compliance could be found for which the airmass consumption was minimal. This optimal compliance is dependent of the imposed trajectory and the physical properties of the pendulum.

The idea behind the compliance controller is to fit the actuator compliance to the natural compliance of the desired trajectory. The natural stiffness of the desired trajectory $K_{trajectory}$, the inverse of the compliance, is calculated as the derivative of the torque $\tilde{T}$ necessary to track the desired trajectory with respect to the joint angle $\tilde{\theta}$. The torque $\tilde{T}$ is given by the inverse dynamics:

$$K_{trajectory} = \frac{d\tilde{T}}{d\tilde{\theta}} = \frac{d}{d\tilde{\theta}}(\hat{D}(\tilde{\theta})\ddot{\tilde{\boldsymbol{\theta}}} + \hat{C}(\tilde{\theta},\dot{\tilde{\theta}})\dot{\tilde{\theta}} + \hat{G}(\tilde{\theta})) \quad (12)$$

where $\hat{D}$ is the inertia matrix, $\hat{C}$ is the centrifugal and coriolis term and $\hat{G}$ is the gravity term, all of these containing estimated values. $\tilde{\theta}$ is the desired trajectory. This stiffness $K_{trajectory}$ is substituted in (11) as a value for K. This is a major change over strategies where an arbitrary compliance value is taken as is the case with most of the robots powered by pneumatic muscles (Schroder et al. 2003; Hildebrandt et al. 2005).

For a pendulum the optimal stiffness $K_{trajectory}$ becomes:

$$\begin{aligned} K_{trajectory} &= \frac{d\tilde{T}}{d\tilde{\theta}} \\ &= \frac{d}{d\tilde{\theta}}\left(d_{11}\ddot{\tilde{\boldsymbol{\theta}}} + g_1\sin(\tilde{\theta})\right) \\ &= d_{11}\frac{\dddot{\tilde{\boldsymbol{\theta}}}}{\dot{\tilde{\boldsymbol{\theta}}}} + g_1\cos(\tilde{\theta}) \end{aligned} \quad (13)$$

with $d_{11} = m\alpha^2 l^2 + I = 0.92$ kg m^2 and $g_1 = gm\alpha l = 23.45$ N m for this pendulum.

For a sinusoidal trajectory $\tilde{\theta} = A\sin(\omega t)$, the optimal stiffness becomes:

$$K_{trajectory} = d_{11}\frac{-A\omega^3\cos(\omega t)}{A\omega\cos(\omega t)} + g_1\cos(A\sin(\omega t)) \quad (14a)$$

$$= -d_{11}\omega^2 + g_1\cos(A\sin(\omega t)) \quad (14b)$$

$$\approx -d_{11}\omega^2 + g_1 \quad (14c)$$

with A the amplitude of the motion, $\omega = 2\pi f$ the angular frequency and f the frequency. The approximation of (14c) is valid if $\tilde{\theta}$ is small. So the optimal stiffness approximates a constant value dependent on the physical properties of the pendulum and the frequency of the imposed motion in case $\tilde{\theta}$ is small.

Table 1 gives the experimentally determined stiffness K_{opt}^{exp} and the calculated natural stiffness of the desired trajectory $K_{trajectory}$ for different frequencies. One can conclude that the calculated stiffness gives a good approximation of the stiffness that is needed in order to reduce air-

Table 1 Experimental and calculated optimal values of K_{opt}

Sine wave frequency (Hz)	$K_{trajectory}^{calculated}$ (N m/rad)	K_{opt}^{exp} (N m/rad) amplitude = 5°	K_{opt}^{exp} (N m/rad) amplitude = 10°
1.5	48	50	50
1.6	59	65	60
1.7	70	80	80
1.8	82	85	85
1.9	95	105	90
2.0	108	125	120
2.1	122	145	125
2.2	137	150	150
2.3	153	150	150
2.4	169		
2.5	186		

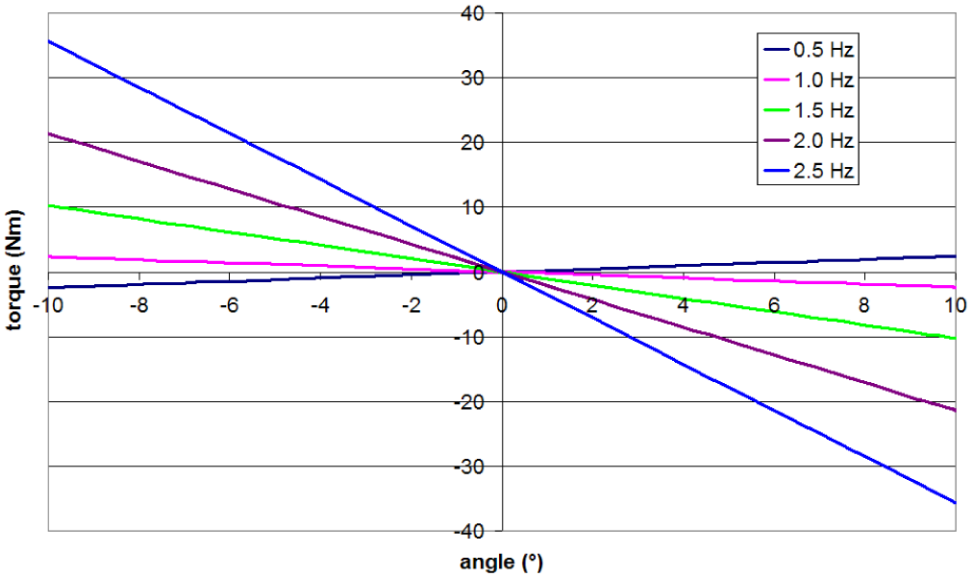

Fig. 11 Torque-angle relation for sinusoidal trajectory for different frequencies

mass consumption. The natural stiffness of the trajectory $K_{trajectory}$ can thus be considered as the optimal stiffness, so $K_{opt} = K_{trajectory}$. At frequencies above 2.2 Hz the optimal stiffness is outside the range the muscles can cover.

Because the optimal stiffness K_{opt} for a sinusoidal function is the derivative of the torque $\tilde{T}$ with respect to the joint angle $\tilde{\theta}$ and that this approximates a constant value. This value can be visualized in a torque-angle graph which for a sine function is a straight line under a certain angle. The slope represents the stiffness. This is shown for different frequencies in Fig. 11. At low frequencies (e.g. 0.5 Hz) the slope of the this curve is positive, the actuator has to generate a positive torque for positive angles to decelerate the pendulum. The reason is that the desired motion is slower than the natural motion. Adapting the stiffness is not valuable here because stiffness can only increase the natural frequency. When the frequency increases the slope of the swing period becomes negative and stiffness adaptation can be used to exploit the natural dynamics.

5 Non-natural trajectories

A sine function is not enough for a walking robot. The joint trajectories deviate from this natural trajectory. A consequence of using a trajectory that is not a sine function is that the natural stiffness of the trajectory is no longer a constant over the trajectory. A first observation is that at some instants $\frac{d\tilde{T}}{d\tilde{\theta}}$ will be infinite or completely stiff. This is of course impossible because the maximum pressure inside the muscles is limited. Before studying a trajectory generated by the trajectory generator, a sum of two sinusoidal functions is presented. The study of this trajectory will provide us some important insights why changing the stiffness over

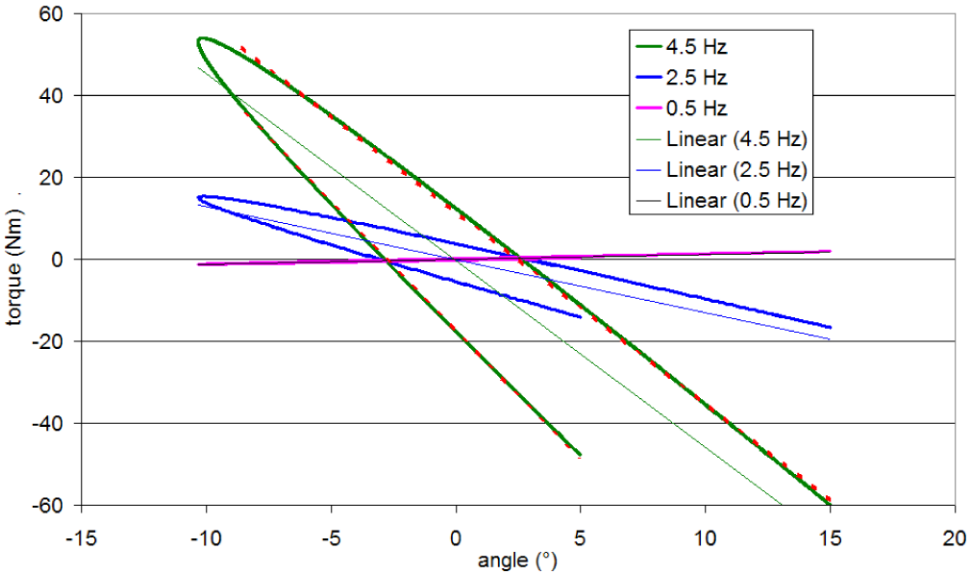

Fig. 12 Torque-angle relation for sum of two sinusoidal trajectories for different frequencies with first order linear regression lines

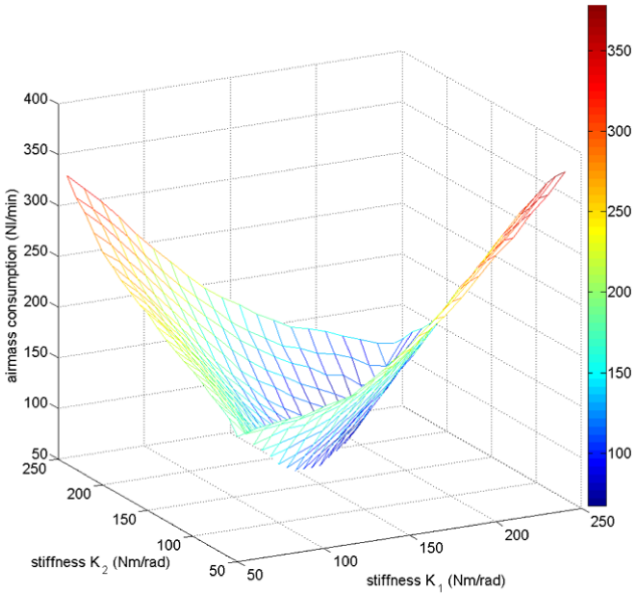

Fig. 13 Power consumption for sum of two sinusoidal trajectories vs stiffness K_1 and K_2 (sim)

the trajectory consumes a lot of energy and that the optimal stiffness will be the average stiffness. Due to the limited capabilities of the pendulum (regarding maximum stiffness and frequency), also simulation results are provided.

5.1 Combination of two sinusoidal functions

The following trajectory is a combination of two sinusoidal functions: $\tilde{\theta} = A\cos(\omega t) + A/2\cos(\omega/2t)$. A is the amplitude and $\omega = 2\pi f$ the angular frequency. The natural stiffness $K_{trajectory}$ of this trajectory is:

$$K_{trajectory} = -d_{11}\omega^2 \frac{\frac{1}{32} + \cos(\omega t/2)}{\frac{1}{8} + \cos(\omega t/2)} + g_{11}\cos(\tilde{\theta}). \quad (15)$$

At $\theta = -10.3°$ the stiffness $K_{trajectory}$ becomes infinite, when the term $\frac{1}{8} + \cos(\omega t/2)$ equals zero. This can also be visualized in Fig. 12, showing the torque-angle relation for different frequencies ranging from 0.5 Hz to 4.5 Hz. At $\theta = -10.3°$ the slope of the tangent at this point is infinite. So tracking $K_{trajectory}$ is impossible. A possible strategy is to choose 2 stiffness values and switch between them. So between $\theta = 5°$ and $\theta = -10.3°$ stiffness K_1 is taken and between $\theta = 15°$ and $\theta = -10.3°$ stiffness K_2. A possibility is that the stiffness of the two red dotted lines shown in Fig. 12 comes out as optimal. In Fig. 13 the airmass consumption for such a trajectory with $A = 10°$ and $f = 3.5$ Hz is given while all the possible combinations are measured for K_1 and K_2 between 50 N m/rad and 250 N m/rad. This is a simulation with extra valves because the real valves cannot follow the desired pressure courses, especially for switching between the desired stiffness values. The valley of minimal airmass consumption is clearly at the values were $K_1 = K_2$. This means that it is not interesting to change the compliance for a certain trajectory. The main reason is that changing the compliance costs energy to increase and decrease the mean pressure $\tilde{p}_s$ and this without delivering torque at the joint. Therefore it will probably be better to select a fixed compliance for a certain repetitive motion and when this motion changes the compliance has to be adapted.

The previous experiment showed that a fixed stiffness setting is preferred above a changing stiffness. The logical next question is which constant stiffness should be selected as optimal? The same combination of two sinusoidal functions

($\tilde{\theta} = A\cos(\omega t) + A/2\cos(\omega/2t)$) is taken with $A = 10°$ and the frequency is increased in steps of 0.25 Hz from 0.5 Hz till 5.25 Hz. Figure 14 shows the airmass consumption versus frequency and stiffness in simulation. A clear minimum is observed for each frequency and the optimal stiffness is plotted in Fig. 16 and called measured optimal stiffness. Under 50 N m/rad and above 200 N m/rad the measured optimal stiffness is meaningless because they are at the borders of the stiffness range. Using Fig. 12 the value of the average stiffness of each frequency is plotted in the same figure. This average stiffness is calculated by taking a first order linear regression of the torque-angle curve (represented by the straight lines), then the slope is the value for the average stiffness. Comparing the measured optimal stiffness to the calculated average stiffness (Fig. 16), one can conclude that the latter serves as a good approximation of the optimal stiffness. A part of this experiment is performed on the real pendulum as shown in Fig. 15. The maximum stiffness is 150 N m/rad and maximum frequency is 2.6 Hz. One can notice that the valley of minimum airmass consumption starts also at 2 Hz as is the case in simulation.

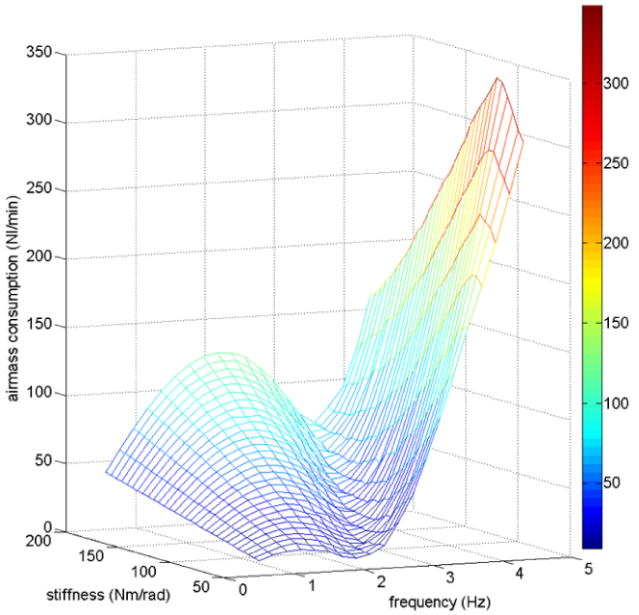

Fig. 14 Airmass consumption for sum of two sinusoidal trajectories vs frequency and stiffness (sim)

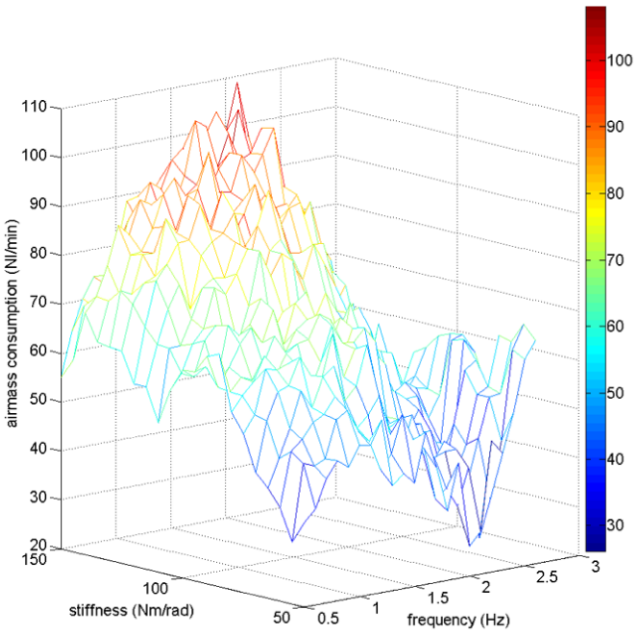

Fig. 15 Airmass consumption for sum of two sinusoidal trajectories vs frequency and stiffness (real)

Fig. 16 Measured and calculated optimal stiffness in function of frequency (sim)

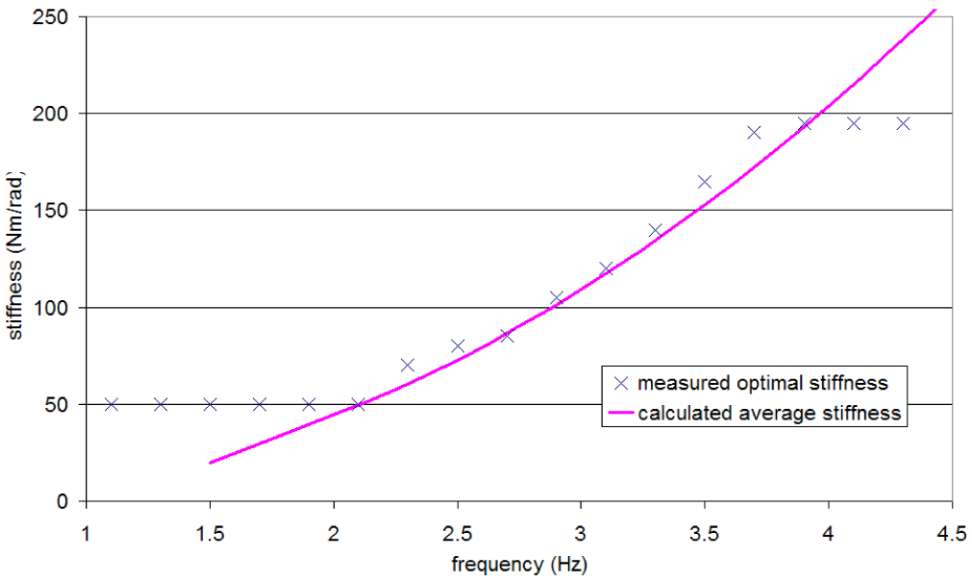

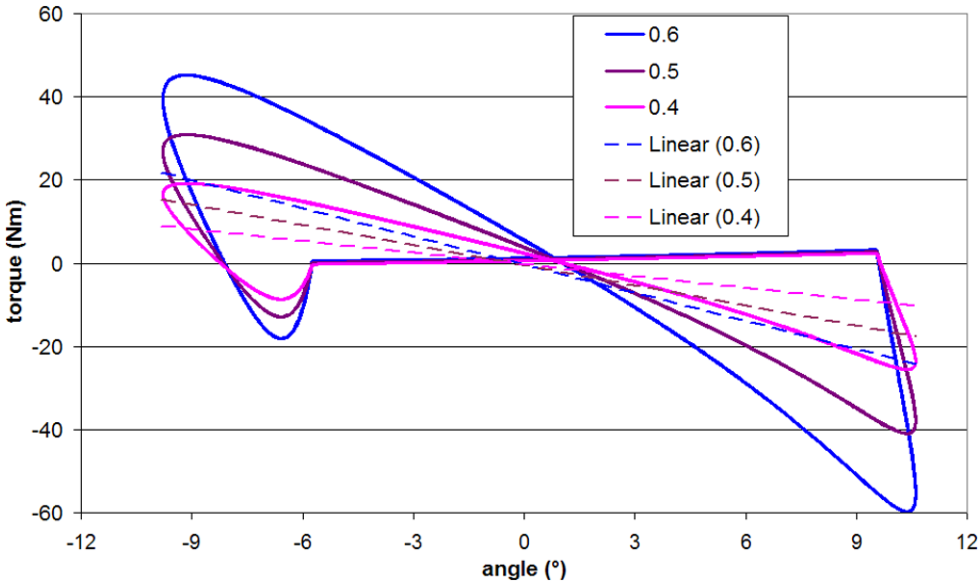

Fig. 17 Torque-angle relation for inverted pendulum hip trajectory for different speeds with first order linear regression lines

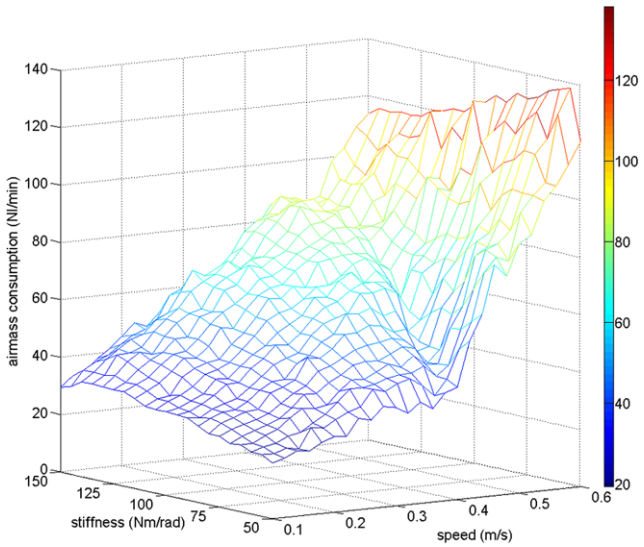

Fig. 18 Airmass consumption vs walking speed and stiffness for hip trajectory (real)

5.2 Hip trajectory

In the following experiments the trajectory for the hip, calculated by a trajectory generator, is imposed as trajectory on the pendulum. In order to generate this motion at higher speeds too, the mass at the end of the pendulum had to be reduced by 3.2 kg (the mass at the end of the pendulum consists of different units so the weight can be easily changed at will). The new physical parameters are $\alpha = 0.66$, $m = 3.58$ kg and $I = 0.08$ kg m^2. Figure 17 shows the computed torque-angle relation for different walking speeds. A remark that has to be made is that the trajectories are generated for walking, but the torques are only for swinging in the air for this specific pendulum. While the actual torques during walking will be different because walking consists of stance phases, double support phases, swing phases and impacts. The airmass consumption is measured for different walking speeds going from $\nu = 0.1$ m/s till $\nu = 0.6$ m/s in steps of 0.02 m/s with a constant step length of $\lambda = 0.2$ m. The stiffness range goes from 50 N m/rad till 150 N m/rad in steps of 5 N m/rad. A valley of minimal airmass consumption can be found which starts from a speed of 0.4 m/s. The minima are not that pronounced anymore. For more complex trajectories, such as a hip trajectory obtained by the trajectory generator, the airmass consumption will increase, because the imposed trajectory differs more from the natural movement of the pendulum. For each walking speed above 0.4 m/s the airmass consumption at the lowest point is about 30% lower than the maximum airmass consumption at that walking speed. The optimal stiffness values for the different walking speeds is plotted in Fig. 19. The minimal stiffness was 50 N m/rad, this explains the flat line between 0.1 m/s and 0.4 m/s. The position of this curve can be explained in a similar way as in the previous case. A first order linear regression has been performed on each curve of the torque-angle relation of Fig. 17 and is shown by a dashed line. The slope of the linear regression line is a stiffness value which is plotted in Fig. 19. One can see that both curves have a similar course. At low walking speeds the motion is slower than the natural motion (average slope is positive) and using compliance is not possible. The strategy is also not applicable when the desired optimal stiffness is less than the stiffness an antagonistic muscle can generate, which is here 50 N m/rad.

So this average stiffness strategy to calculate the optimal stiffness seems to be interesting to apply. An advantage of

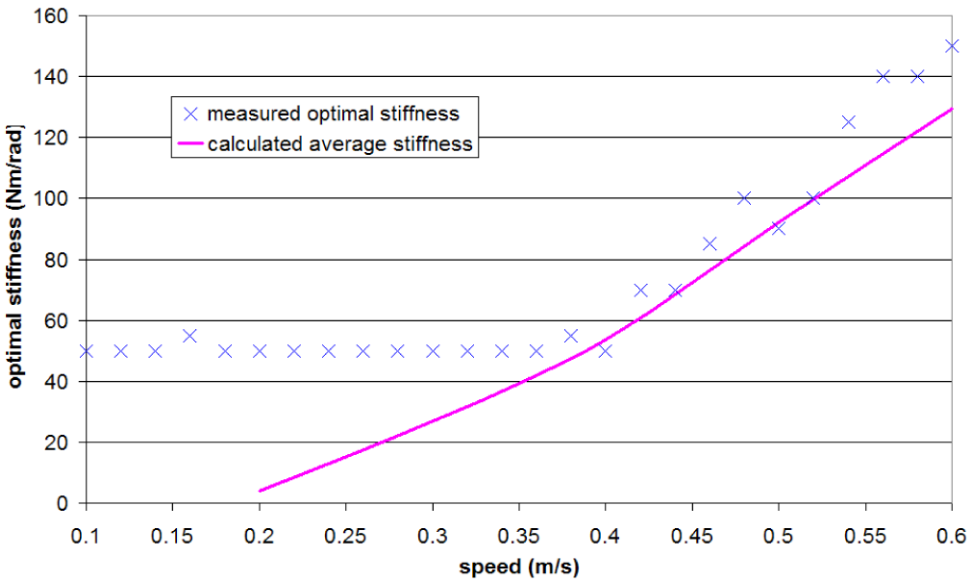

Fig. 19 Optimal compliance in function of walking speed (real)

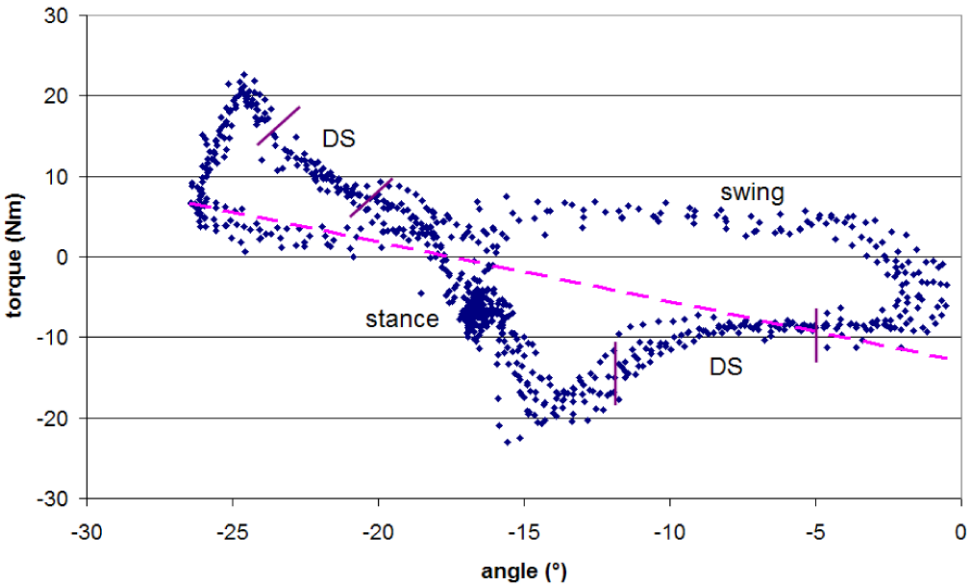

Fig. 20 Torque-angle relation of hip joint for real walking with first order linear regression line (real)

this strategy is that it is also applicable to other designs of passive compliant actuators, for example MACCEPA (Van Ham et al. 2007), AMASC (Hurst et al. 2004), VSA (Bicchi and Tonietti 2004) or MARIONET (Sulzer et al. 2005). The complete strategy calculates a torque T so a desired trajectory is tracked and a stiffness K so the energy consumption is minimized. These are provided as input to the compliant actuator. Using (9a) and (9b) together with (10) and (11) the pressures inside the muscles can be calculated if an antagonistic setup of two muscles is used as compliant actuator.

Figure 20 depicts the torque-angle relation of the hip joint for the real walking robot Lucy. When the average stiffness strategy of the torque-angle relation of the hip of the walking robot is calculated, a stiffness of 42 N m/rad is obtained. This is lower than the minimal attainable stiffness. In other words, the maximum walking speed of the robot is too slow to have the optimal stiffness lying in the feasible stiffness range. So, for now it is not sensible to implement this strategy in the real biped, due to its current walking speed limitation.

Experiments concerning compliance adaptation have also been performed on the walking robot WL-14. A reduction of 25% of energy consumption during the swing phase was observed compared to the case when the stiffness was not varied actively (Yamaguchi et al. 1998). This was measured when walking at 1.28 s/step and 0.15 m/step. Strategies on how the optimal stiffness was chosen were not discussed.

6 Conclusion

Actuators with adaptable compliance are gaining interest in the field of robotics. Little research, however, has been carried out on how to control the compliance. In this work a study is performed considering adapting the natural dynamics by compliance control and evaluated on a single pendulum structure. It was shown that for sine trajectories an optimal stiffness can be found with minimal energy consumption. A strategy was proposed to find this optimal compliance. The idea behind the mathematical formulation is to fit the controllable stiffness of the actuator to the natural stiffness of the desired trajectory. A first more complex trajectory that has been studied is a sum of two sinusoidal functions. Experiments showed that changing the stiffness during the trajectory costs a lot of energy. This should be avoided and therefore a strategy with a fixed stiffness for a certain trajectory is preferable. A good approximation of the optimal stiffness is the slope of the first order linear regression line of the torque-angle curve. This average stiffness strategy also proved itself useful when a hip trajectory, as calculated by the trajectory generator, is considered as the imposed trajectory. The minima were not that distinct anymore, as for more complex trajectories the energy consumption increases due to the fact that these trajectories deviate from the unforced motion to a greater extent.

The strategy is not yet implemented in the real biped Lucy. The current maximum walking speed is too low to use the proposed average stiffness strategy for exploiting the natural dynamics. Another important remark is the fact that the trajectory generator for the biped Lucy is not yet able to incorporate compliance adaptation. At this moment the strategy is to generate the trajectories first so the dynamic stability is guaranteed and executing the compliance control afterwards. An improvement is that the trajectory generator is optimized towards energy-consumption and that the compliant characteristics of the actuator are incorporated.

Acknowledgements The author B. Vanderborght is a post-doc researcher with a grant from the Fund for Scientific Research-Flanders (Belgium) (FWO). Lucy has been built with the financial support of the Research Council (OZR) of the Vrije Universiteit Brussel.

References

Basmajian, J., & De Luca, C. (1985). *Muscles alive: their function revealed by electromyography* (p. 1964).

Bicchi, A., & Tonietti, G. (2004). Fast and soft arm tactics: dealing with the safety-performance trade-off in robot arms design and control. In *IEEE robotics and automation magazine* (Vol. 11, pp. 22–33).

Bicchi, A., Tonietti, G., Bavaro, M., & Piccigallo, M. (2003). Variable stiffness actuators for fast and safe motion control. In *International symposium robotics research* (pp. 100–110).

Caldwell, D., Medrano-Cerda, G., & Bowler, C. (1997). Investigation of bipedal robot locomotion using pneumatic muscle actuators. In *IEEE international conference on robotics and automation (ICRA 1997)* (pp. 799–804).

Collins, S. H., Ruina, A., Tedrake, R., & Wisse, M. (2005). Efficient bipedal robots based on passive-dynamic walkers. *Science*, *18*(307), 1082–1085.

Daerden, F., & Lefeber., D. (2001). The concept and design of pleated pneumatic artificial muscles. *International Journal of Fluid Power*, *2*(3), 41–50.

Davis, S., Tsagarakis, N., Canderle, J., & Caldwell, D. G. (2003). Enhanced modelling and performance in braided pneumatic muscle actuators. *The International Journal of Robotic Research*, *22*(22), 213–227.

Ferris, D. P., & Farley, C. T. (1997). Interaction of leg stiffness and surface stiffness during human hopping. *Journal of Applied Physiology*, *82*(1), 15–22.

Gorce, P., & Guihard, M. (1998). On dynamic control of pneumatic bipeds. *Journal of Robotic Systems*, *15*(7), 421–433.

Guccione, S., Muscato, G., & Spampinato, G. (2003). A human inspired robotic leg: design, control and mechanical realization. In *IEEE international conference on humanoid robots*.

Hildebrandt, A., Sawodny, O., Neumann, R., & Hartmann, A. (2005). Cascaded control concept of a robot with two degrees of freedom driven by four artificial pneumatic muscle actuators. In *American control conference* (Vol. 1, pp. 680–685).

Honda Motor Co., Ltd. (2005). New asimo—running at 6 km/h. http://world.honda.com/HDTV/ASIMO/New-ASIMO-run-6kmh/.

Hurst, J. W., Chestnutt, J., & Rizzi, A. A. (2004). An actuator with physically variable stiffness for highly dynamic legged locomotion. *IEEE international conference on robotics and automation (ICRA 2004)* (pp. 4662–4667), New Orleans, USA.

Kajita, S., Kanehiro, F., Kaneko, K., Fujiwara, K., Harada, K., Yokoi, K., & Hirukawa, H. (2003). Biped walking pattern generation by using preview control of zero-moment point. In *IEEE international conference on robotics and automation (ICRA 2003)* (Vol. 2, pp. 1620–1626).

Kato, I., Mori, Y., & Masuda, T. (1972). Pneumatically powered artificial legs walking automatically under various circumstances. In *Proceedings of the 4th international conference on external control of human extremities* (pp. 458–470).

Kuo, A. D., Donelan, J. M., & Ruina, A. (2005). Energetic consequences of walking like an inverted pendulum: step-to-step transitions. *Exercise and Sport Sciences Reviews*, *33*(2), 88–97.

Michel, P., Chestnutt, J., Kuffner, J., & Kanade, T. (2005). Vision-guided humanoid footstep planning for dynamic environments. In *IEEE-RAS international conference on humanoid robots* (pp. 13–18).

Schroder, J., Erol, D., Kawamura, K., & Dillman, R. (2003). Dynamic pneumatic actuator model for a model-based torque controller. In *IEEE international symposium on computational intelligence in robotics and automation (CIRA 2003)* (Vol. 1, pp. 342–347).

Schulte, H. F. (1961). The characteristics of the McKibben artificial muscle. In *The application of external power in prosthetics and orthotics* (pp. 94–115). Lake Arrowhead: National Academy of Sciences–National Research Council.

Slotine, J. J. E., & Li, W. (1991). *Applied nonlinear control*. Cambridge: Prentice-Hall.

Sulzer, J., Peshkin, M., & Patton, J. (2005). MARIONET: an exotendon-driven, rotary series elastic actuator for exerting joint torque. In *International conference on robotics for rehabilitation (ICORR 2005)* (pp. 103–108).

Van Ham, R., Vanderborght, B., Van Damme, M., Verrelst, B., & Lefeber, D. (2007). MACCEPA, the mechanically adjustable compliance and controllable equilibrium position actuator: design and implementation in a biped robot. *Robotics and Autonomous Systems*, *55*(10), 761–768.

Vanderborght, B., Verrelst, B., Van Ham, R., & Lefeber, D. (2006a). Controlling a bipedal walking robot actuated by pleated pneumatic artificial muscles. *Robotica*, *24*(04), 401–410.

Vanderborght, B., Verrelst, B., Van Ham, R., Van Damme, M., Lefeber, D., Meira, Y., Duran, B., & Beyl, P. (2006b). Exploiting natural dynamics to reduce energy consumption by controlling the compliance of soft actuators. *The International Journal of Robotics Research*, *25*(4), 343–358.

Verrelst, B., Van Ham, R., Vanderborght, B., Daerden, F., & Lefeber, D. (2005). The pneumatic biped LUCY actuated with pleated pneumatic artificial muscles. *Autonomous Robots*, *18*, 201–213.

Verrelst, B., Stasse, O., Yokoi, K., & Vanderborght, B. (2006a). Dynamically stepping over obstacles by the humanoid robot HRP-2. In *IEEE-RAS international conference on humanoid robots* (pp. 117–123).

Verrelst, B., Van Ham, R., Vanderborght, B., Lefeber, D., Daerden, F., & Van Damme, M. (2006b). Second generation pleated pneumatic artificial muscle and its robotic applications. *Advanced Robotics*, *20*(7), 783–805.

Walker, R. (1996). Using air muscles for compliant bipedal and many-legged robotics. In *IEE colloquium on information technology for climbing and walking robots* (pp. 3/1–3/3).

Yamaguchi, J., Nishino, D., & Takanishi, A. (1998). Realization of dynamic biped walking varying joint stiffness using antagonistic driven joints. In *IEEE international conference on robotics and automation (ICRA 1998)* (Vol. 3, pp. 2022–2029).

Yoshida, E., Esteves, C., Sakaguchi, T., Laumond, J.-P., & Yokoi, K. (2006). Smooth collision avoidance: practical issues in dynamic humanoid motion. In *IEEE/RSJ international conference on intelligent robots and systems (IROS 2006)* (pp. 827–832).

Bram Vanderborght was born in Wilrijk, Belgium, in 1980. He received the degree in study of Mechanical Engineering at the Vrije Universiteit Brussel in 2003. Since 2003 he was researcher at the Vrije Universiteit Brussel, supported by the Fund for Scientific Research Flanders (FWO). In May 2007 he received his PhD in Applied Sciences. The focus of his research is the use of adaptable compliance of pneumatic artificial muscles in the dynamically balanced biped Lucy. In May 2006 he performed research on the humanoids robot HRP-2 at the Joint Japanese/French Robotics Laboratory (JRL) in AIST, Tsukuba (Japan) in the ongoing research "Gait Planning for Humanoids Robots: Negotiating Obstacles". From October 2007 he will work as post-doc researcher at the Italian Institute of Technology in Genua, Italy.

Björn Verrelst was born in Antwerp, Belgium, in 1972. He received the degree in study of Mechanical Engineering at the Vrije Universiteit Brussel in 1996 and a PhD in Applied Sciences in 2005. Currently he is Post-doc researcher at the Vrije Universiteit Brussel. The focus of his research is the use of pneumatic artificial muscles in the walking biped Lucy for dynamically balanced walking and compliant actuation for robotic applications in general. During the period 2005/2006 he conducted a one year JSPS post-doc research at the National Institute for Advanced Industrial Science and Technology in Tsukuba, Japan.

Ronald Van Ham was born in Bonheide, Belgium, in 1976. He received the degree in study of Electro-Mechanical Engineering at the Vrije Universiteit Brussel in 1999 and a PhD in Applied Sciences in 2006. He participated in the research towards the biped Lucy and developed the MACCEPA, a novel compliant actuator and the biped Veronica.

Michaël Van Damme was born in 1978. He received the degree in study of Electrical Engineering at the Vrije Universiteit Brussel in 2001. He is researcher and teaching assistant at the Vrije Universiteit Brussel since 2003. The focus of his research is the use of a robotic assistive device in direct contact with an operator.

Pieter Beyl was born in Anderlecht (Brussels, Belgium) in 1982. He received the master of science degree in mechanical engineering from Vrije Universiteit Brussel in 2005. Currently, he's a researcher and teaching assistant. His research is in the area of medical rehabilitation robotics, aiming at the design, construction and control of a step rehabilitation robot.

Dirk Lefeber was born in 1956. He received the degree in Study of Civil Engineering at the Vrije Universiteit Brussel and a PhD in Applied Sciences, Vrije Universiteit Brussel, in 1986. Currently he is professor at the dept. of Mechanical Engineering and head of the Robotics and Multibody Mechanics Research Group, Vrije Universiteit Brussel. His research interests are new actuators with adaptable compliance, dynamically balanced robots, robot assistants, rehabilitation robotics and multibody dynamics.